Research Article

Roland Tolulope Loto*

Corrosion polarization and passivation behavior of selected stainless steel alloys and Ti6Al4V titanium in elevated temperature acid-chloride electrolytes

https://doi.org/10.1515/eng-2022-0052 received November 07, 2021; accepted June 23, 2022

Abstract: The corrosion polarization behavior of 439ll ferritic (43911), 316L austenitic (316L), and NO7208 nickelchromium-aluminum-iron (NO7208) stainless steels, and Ti6Al4V titanium (Ti6Al4V) allovs was studied in 4 M H₂SO₄ + 5% NaCl solution at 35 and 70°C. Corrosion rate (C_R) of the alloys were generally higher at 70°C. NO7208 and 439ll alloy exhibited higher resistance to general corrosion at 35°C (0.067 and 0.050 mm/year) while Ti6Al4V was the most reactive (0.506 mm/year). Passivation behavior was evident on the plots of NO7208 and Ti6Al4V alloys. NO7208 pitted at 1.04 V with passivation range of 0.17 V. Metastable pitting occurred at 0.02 V and ceased at 0.19 V. Pitting was absent from the polarization plot of Ti6Al4V though it exhibited metastable pitting at -0.39 V and passivated at -0.21 V. At 70°C, NO7208 alloy exhibited the lowest C_R (0.392 mm/year), while Ti6Al4V was the most reactive at 21.868 mm/year. $C_{\rm R}$ of the alloys increased by 97.63%, 91.18%, 82.83%, and 97.69% at 70°C. Corrosion potential of the alloys shifted cathodically at 35 and 70°C signifying dominant cathodic processes. Ti6Al4V exhibited passivation behavior at 70°C with no pitting evidence. Open circuit potential measurement showed that Ti6Al4V was the most electronegative and NO7208 alloy was the most electropositive due to the significant growth of its protective oxide. Grain boundary corrosion was visible on 4391l and 316L at 35°C and total surface deterioration at 70°C. Pseudo corrosion pits were visible on NO7208 and Ti6Al4V alloy at 35°C. At 70°C, total surface degradation was visible on Ti6Al4V and grain boundary corrosion on NO7208.

Keywords: corrosion management, passivation, steel, titanium, pitting, environmental degradation

1 Introduction

Demand for cost effective and highly corrosion resistant alloys in astringent environments at room and elevated temperature is of utmost importance due to the long-term cost advantages, prolonged service life, and decrease in maintenance cost. Industrial operating conditions in petrochemical plants, chemical processing industry, fertilizer production, desalination, heat exchangers, manufacture of intermediate chemicals, marine application, energy generation, automobiles etc., consists of, and release reactive anions detrimental to the functional lifespan of metallic alloys. The anions are responsible for moderate to accelerated deterioration of the alloys. This deterioration phenomenon is scientifically known as corrosion. Corrosion is broadly interpreted as the chemical or electrochemical interaction of metallic alloys with their operating environments resulting in the deterioration of their physical, mechanical, metallurgical, microstructural, and aesthetic properties. The inherent tendency of metallic alloys to return to their original state of lower energy in the form of ores is responsible for the reaction [1-6]. Metallic alloys such as ferritic stainless steels, austenitic stainless steel, martensitic alloy, nickel chromium alloys, titanium alloys etc., are broadly utilized in corrosive environments where carbon steels, low grade alloys, and general 304 stainless steels are unable to survive for extended periods. Resistance of stainless steels to corrosion results from the evolution of an unreactive film on the steel exterior. The strength and properties of the protective oxide is a product of microstructural and metallurgical properties of the alloys, and the quantitative presence of some important alloying elements.

^{*} Corresponding author: Roland Tolulope Loto, Department of Mechanical Engineering, Covenant University, Ota, Ogun State, Nigeria, e-mail: tolu.loto@gmail.com

However, under certain conditions with respect to reactive anion concentration and their combinations in addition to elevated temperatures, the protective oxide of metallic alloys, undergo repetitive active-passive transition behavior, crack propagation, thinning, and under extreme cases immediate collapse. This results in general and localized corrosion of the alloys. Localized corrosion of metallic alloys is a major industrial problem due to their insidious nature, difficulty in detection, and severe compromise of structural integrity [7-13]. In petrochemical plants, localized corrosion is responsible for a substantial damage of metallic allovs eventually being responsible for lost production, epileptic operation, and excessive cost of repairs and replacement. During petrochemical operations, corrosion due to hydrolysis of salts accelerates the deterioration of the alloy in operation. Hydrogenation is another consequence resulting in impairment of their mechanical properties [14,15]. Elevated temperature applications of metallic alloys are directly accountable for the priority given to the selection of appropriate metallic alloys for specific industrial applications. High temperature operating environments enhance the reactivity of anionic molecules which in turn are aggressive to the surface integrity of metallic alloys resulting in the formation of oxides, carbides, sulfides, etc. These causes the prevalent equipment failure and decline in machine and equipment reliability and functional lifespan [16]. The resistance of the protective oxide on metallic alloys in high temperature operating conditions is of utmost importance [17,18]. Investigation has demonstrated that high temperature significantly determines the passivation characteristics of metallic alloys [19,20]. However, it is worthy of note that the combined effects of high temperature and high anionic concentration are deleterious to the corrosion resilience of metallic alloys and resilience of their protective oxides. The kinetics of the protective oxide evolution and growth is subject to the rate constants of the surface reactions of anionic species and diffusion through the oxide which can be exacerbated by high temperature e.g., 2205 duplex stainless is resistant to Cl⁻ anionic stress-corrosion cracking in non-complex NaCl media at 665°C [21,22]. One of the major consequences of a weakened protective oxide is the initiation and growth of corrosion pits [23–27]. Corrosion pits are often difficult to recognize leading to leaks, damaging fractures, and catastrophic breakdowns. Hence the significance of more assessment of the corrosion resistance of metallic alloys. 439ll ferritic steel (439ll) is extensively applied where oxidation and corrosion resistance are of utmost importance such as tubular manifolds and exhaust system components, food processing industries, and breweries. Nickel chromium aluminum iron (NO7208) is an age-hardened

nickel-based superalloy that combines excellent creep strength with thermal stability, weldability, and fabricability. It is used in the manufacture of air and land-based turbines, airplane exhaust nozzles as well as high temperature automotive gaskets and seals. 316L austenitic stainless steel (316L) is a marine grade stainless steel with lower carbon content than 316 steel. It is applied in marine environments, chemical processing industry, food production, manufacture of pharmaceutical equipment, and wastewater treatment. Ti6Al4V titanium alloy (Ti6Al4V) is an $\alpha + \beta$ titanium alloy which combines high strength with low density, high fracture toughness, excellent corrosion resistance, and superior biocompatibility. It is used in the production of aerospace parts, gas turbines, in chemical processing and marine applications, and additive manufacturing. This study focuses on the electrochemical characteristics of 439ll, 316L, NO7208, and Ti6Al4V titanium alloy in 4 M H₂SO₄ + 5% NaCl solution at 35 and 70°C. Emphasis is given to the passivation behavior and localized corrosion reaction of the alloys within the electrolyte.

2 Experimental procedure

2.1 Materials preparation

439ll, 316L, NO7208, and Ti6Al4V obtained from McMaster University, Ontario, Canada, Vienna University of Technology, Vienna, Austria, and University of Johannesburg, Johannesburg, South Africa were analyzed with Phenom ProX Scanning Electron Microscope (Model No. MVE0224651193) at the Central Laboratory, Covenant University to identify their elemental composition. The nominal (wt%) constituent of the alloys are presented in Table 1. 439ll, 316L, NO7208, and Ti6Al4V alloys were cut using hacksaw into 2 samples each, totaling 8 samples with dimensions of $3 \text{ mm} \times 5 \text{ mm}$ (length × breadth). A Cu wire was attached to the alloy samples using a soldering iron and the samples were embedded in pre-hardened resin mixture. The exposed area of the embedded samples was thereafter grinded with sandpaper of 80, 120, 220, 600, and 1,000 grit sizes according to ASTMG59-97 [28], burnished with 6 µm diamond polishing solution, and later sanitized with deionized H₂O and C₃H₆O in accordance with ASTM G1-03 [29].

2.2 Test solution

Conventional grade recrystallized NaCl (obtained from Loba Chemie PVT. Ltd, India) was concocted into cubic

Element	Р	S	С	Cr	Ni	Al	Mn	Ti	Fe	Мо	Si	Со	0	Н	N	Υ	٧
Ti6Al4V																	
% Comp. 439ll	-	-	0.08	-	_	6	_	89.35	0.3	-	-	-	0.2	0.015	0.05	0.005	4
% Comp. 316L	0.04	0.03	0.03	19	0.5	0.15	1	0.5	77.72	_	1	-	_	-	0.03	_	-
% Comp. NO7208	0.045	0.03	0.03	18	13	-	2	-	62.9	3	1	_	-	-	-	-	-
% Comp.	_	_	0.06	20	56	1.5	0.3	2.1	1.5	8.5	0.15	10	_	_	_	_	_

Table 1: Nominal (wt%) constituent of 439ll, 316L, NO7208, and Ti6Al4V alloy

concentrations of 5% in 400 mL of 4 M H_2SO_4 solution by adding 20 g NaCl into a beaker, filling up to 400 mL of the required dilute H_2SO_4 solution concentration. Dilute H_2SO_4 was prepared from conventional grade reagent of the acid (98%, purchased from Sigma Aldrich, USA).

2.3 Electrochemical test

Potentiodynamic polarization tests were performed at 35 and 70°C with a ternary electrode configuration within a transparent beaker containing the acid-chloride electrolyte (placed on a portable heating device) and a thermometer using Digi-Ivy 2311 electrochemical device plugged to a computer system. Polarization curves were plotted at sweep rate of 0.0015 V/s from -0.8 to +1.75 V in accordance with ASTM G102-89(2015) [30]. $C_{\rm D}$ ($C_{\rm D}$, A/cm²) and corrosion potential ($C_{\rm P}$, V) values were determined by the Tafel extrapolation technique. Corrosion rate ($C_{\rm R}$) was determined as indicated below:

$$C_{\rm R} = \frac{0.00327^* C_{\rm D}^* E_{\rm Q}}{D},\tag{1}$$

where $E_{\rm Q}$ represents the sample equivalent weight (g). 0.00327 represents $C_{\rm R}$ constant [31]. Open circuit potential (OCP) analysis was executed at 0.2 V/s step potential for 5,400 s to analyze the active/passive reaction and thermodynamic state of the alloys in 4 M H₂SO₄ + 5% NaCl solutions at 35 and 70°C [32].

2.4 Optical microscopy characterization

Optical representative images of 439ll, 316L, NO7208, and Ti6Al4V alloy surfaces in $4\,M\,H_2SO_4 + 5\%$ NaCl solution at 35 and 70°C were studied and compared using Omax microscope.

3 Results and discussion

3.1 Potentiodynamic polarization studies

The corrosion polarization behavior of 439ll, 316L, NO7208, and Ti6Al4V alloys in 4 M H₂SO₄ + 5% NaCl solution at 35 and 70°C are shown in Figure 1a and b. Data (C_R , C_D , $C_{\rm P}$, polarization resistance, and cathodic and anodic Tafel slopes) obtained from the polarization plots are revealed in Table 2. 439ll, NO7208, and 316L alloys exhibited similar cathodic polarization slope configuration (Figure 1a) indicating that the mechanism of H₂ evolution and O₂ reduction reaction are similar at 35°C. Second the alloys react similarly with respect to activation control mechanisms. This is established from the close relationship between the $C_{\rm P}$ values in Table 2 which differ from -0.208 and -0.288 V, indicating that the mechanism of the redox electrochemical processes are similar. The plot configuration of the cathodic polarization slope of Ti6Al4V differs from the ferrous alloys indicating that the mechanism of cathodic reaction differs. Hence, its C_P of $-0.496\,\mathrm{V}$ varies significantly from the corresponding potential values of the ferrous alloys. The general cathodic reaction mechanisms are shown in the following equations [33]:

$$2H_2O + 2e^- \rightarrow H_2 + 2OH^-,$$
 (2)

$$2H^+ \rightarrow 2H - 2e^- \rightarrow H_2 - 2e^-,$$
 (3)

$$O_2 + 4H^+ + 4e^- \rightarrow H_2O_*$$
 (4)

Inspection of the C_R outputs in Table 2 shows that 439ll which exhibited the least C_R of 0.050 mm/year analogous to C_D and polarization resistance of 4.63×10^6 A/cm² and 5,545 Ω , respectively, is the most resistant to general corrosion, while Ti6Al4V displays the highest general C_R result at 0.506 mm/year corresponding to polarization resistance of 589.5 Ω . Corrosion of the metallic alloys is caused by the electrochemical action of SO_4^{2-} and

514 — Roland Tolulope Loto DE GRUYTER

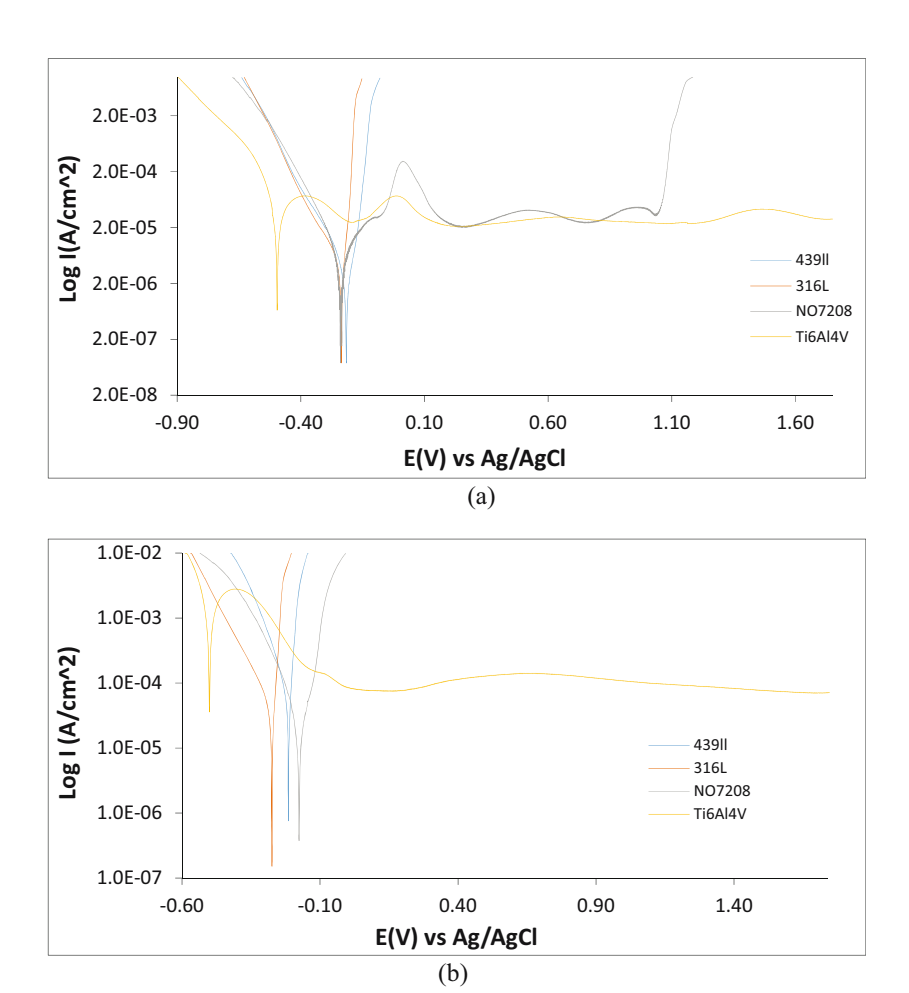


Figure 1: Corrosion polarization plots of 439ll, 316L, NO7208, and Ti6Al4V alloys in 4 M H₂SO₄ + 5% NaCl solution at (a) 35°C and (b) 70°C.

Table 2: Corrosion polarization data for 439ll, 316L, NO7208, and Ti6Al4V alloys in 4 M H₂SO₄ + 5% NaCl solution at 35 and 70°C

Sample	C _R (mm/year)	Corrosion current (A)	$C_{\mathrm{D}}~(\mathrm{A/cm^2})$	$C_{P}(V)$	Polariza resistan	tion ce, $R_{ m p}~(\Omega)$	Cathodic Tafel slope, B_c (V/dec)	Anodic Tafel slope, <i>B</i> _a (V/dec
35°C								
439ll	0.0050	4.63×10^{-6}	4.63×10^{-6}	-0.208	5545.0		-7.992	43.290
316L	0.100	9.31×10^{-6}	9.31×10^{-6}	-0.288	2761.0		-6.714	12.110
NO7208	0.067	6.45×10^{-6}	6.45×10^{-6}	-0.235	3987.0		-9.433	5.268
Ti6Al4V	0.506	4.36×10^{-5}	4.36×10^{-5}	-0.496	589.5		-9.145	2.341
Sample	C _R (mm/year)	% Change in C _R	Corrosion current (A)	C _D (A/cm ²)	<i>C</i> _P (V)	Polarization Resistance, $R_{\rm p}~(\Omega)$	Cathodic Tafel slope, B_c (V/de	Anodic Tafel c) slope, B _a (V/dec)
70°C								
439ll	2.099	97.63	1.95×10^{-4}	1.95×10^{-4}	-0.210	131.50	-11.53	2.911
316L	1.134	91.18	1.06×10^{-4}	1.06×10^{-4}	-0.270	243.50	-8.262	3.317
NO7208	0.392	82.83	3.75×10^{-5}	3.75×10^{-5}	-0.172	684.70	-9.624	33.150
Ti6Al4V	21.868	97.69	1.89×10^{-3}	1.89×10^{-3}	0.504	13.63	-6.559	1.552

 ${
m Cl}^-$ species which adsorb at weak regions on 439ll, 316L, and NO7208 alloy surfaces during redox reactions resulting

in an intermediate complex, and invariably the accelerated collapse of their protective film [34,35]. The following

equations describe the corrosion processes of the ferrous alloys [36,37];

$$Fe + H_2SO_4 \rightarrow FeSO_4 + H_2,$$
 (5)

(7)

Fe +
$$2NaCl + 2H_2O \rightarrow H_2 + FeCl_2 + 2NaOH$$
, (6)

$$Cr_2O_3 + H_2SO_4 \rightarrow Cr_2(SO_4)_3 + H_2O_4$$

$$Cr_2O_3 + 6NaCl \rightarrow 2CrCl_3 + 3Na_2O.$$
 (8)

 C_R of Ti6Al4V is due to the accelerated deterioration of the inert film on its surface. In accordance with the reaction equation below, Ti6Al4V oxidizes in the acid-chloride electrolyte to Ti³⁺ and discharges therein:

$$Ti \rightarrow Ti^{3+} + 3e^{-}$$
. (9)

The protective film on Ti6Al4V evolves due to the growth of TiO_2 , with respect to the equation below [38,39]:

$$Ti + O_2 \rightarrow TiO_2$$
. (10)

 ${
m TiO_2}$ is a product of the reaction between Ti6Al4V and adsorbed ${
m O_2}$. Dissolution of TiO₂ is assumed to occur owing to the combined reaction effect of ${
m SO_4}^{2-}$ and ${
m Cl}^-$ anions which consequentially hinders the growth of the protective film by chemically displacing the adsorbed ${
m O_2}$ and through the substitutional process of competitive adsorption. ${
m SO_4}^{2-}$ tends to complex with ${
m Ti}^{4+}$ enhancing its corrosion [40,41]. ${
m TiO_2}$ reacts with ${
m Cl}^-$, ${
m SO_4}^{2-}$, and ${
m O_2}$ (equations (6)–(8)) [42] within the electrolyte according to the following equations:

$$2Ti + 3H_2SO_4 \rightarrow Ti_2(SO_4)_3 + 3H_2,$$
 (11)

$$5\text{TiO}_2 + 4\text{NaCl} + \text{O}_2 \rightarrow \text{Na}_4\text{Ti}_5\text{O}_{12} + 2\text{Cl}_2,$$
 (12)

$$6\text{TiO}_2 + 4\text{NaCl} \rightarrow \text{Na}_4\text{Ti}_5\text{O}_{12} + \text{TiCl}_4. \tag{13}$$

 Cl^- anion reacts with substrate Ti6Al4V [43,44], significantly contributing to the collapse of the protective oxide (equations (9)–(13)).

$$5\text{TiO}_2 + 4\text{NaCl} + 2\text{H}_2\text{O} \rightarrow \text{Na}_4\text{Ti}_5\text{O}_{12} + 4\text{HCl},$$
 (14)

$$TiCl_4 + 2H_2O \rightarrow TiO_2 + 4HCl,$$
 (15)

$$2HCl + Ti \rightarrow TiCl_2 + H_2, \tag{16}$$

$$4HCl + Ti \rightarrow TiCl_4 + 2H_2, \tag{17}$$

$$2\text{TiCl}_2 + O_2 + 2\text{H}_2\text{O} \rightarrow 2\text{Ti}O_2 + 4\text{HCl}.$$
 (18)

However, findings from other investigations show that during the redox reaction processes, several reaction mechanism occurs simultaneously [45–47]. In the presence of $\rm Cl^-$ anions, $\rm SO_4^{2-}$ anions are inclined to exhibit inhibiting effect on the stability of passive films due to competitive adsorption between the anions in interaction with the alloy at the passive film–electrolyte layer. This

leads to a pseudo protected but highly reactive metallic surface [48–50].

It must be noted that the C_P values in Table 2 at 35°C corresponds to the C_R of the metallic alloys. The more electronegative the C_P , i.e., the greater the degree of cathodic shift, the higher the C_R of the alloy. This signifies that the cathodic reaction mechanisms strongly influence the corrosion resistance of the alloys inside the acidchloride electrolyte. Increase in experimental temperature from 35 to 70°C significantly increased the C_R of the alloys. The percentage variation ranges from 82.83 to 97.69%. Ti6Al4V exhibited the highest percentage variation in C_R with a value of 21.868 mm/year at 70°C. However, NO7208 exhibited the lowest percentage change in C_R signifying the highest resistance to corrosion in mildly high temperature operating conditions with C_R output of 0.392 mm/year. The C_P values show 439ll and Ti6Al4V alloy further shifted to cathodic potentials at 70°C, while 316L shifted to anodic values signifying dominant anodic dissolution reaction processes. At this point, the mechanism of cathodic reaction processes generally differs as shown in the cathodic polarization plot configuration. C_R of Ti6Al4V shows that it is the most vulnerable to general corrosion at high temperature in extreme process environment.

3.2 Potentiostatic studies

Potentiostatic studies of the localized corrosion resilience of NO7208 and Ti6Al4V metallic alloys were studied. The protective oxide of NO7208 and Ti6Al4V metallic alloys were exceptionally resistant to the corrosive reactions of SO_{4}^{2-} and Cl^{-} anions especially at 35°C. The properties of the protective oxide are subject to the concentration of the anions and electrolyte temperature [51-54]. Metastable pitting activity and passivation behavior were missing from the polarization plot of 439ll and 316L alloys due to the collapse of their passive protective films through mechanisms earlier proposed by other authors following anodic polarization compared to NO7208 and Ti6Al4V [55–62]. The electrochemical action of SO_4^{2-} and Cl⁻ anions completely destroyed their protective oxide and prevented their reformation during the redox electrochemical process. The anions transit from the metal filmelectrolyte layer to the metal-film layer, dominating the reaction mechanism therein. The reaction mechanisms were further exacerbated by the overwhelming concentration of anions. Table 3 shows the potentiostatic data for NO7208 and Ti6Al4V alloys in 4 M H₂SO₄ + 5% NaCl

Fable 3: Potentiostatic data for NO7208 and Ti6Al4V metallic alloys in 4 M $_{
m 4}$ SO $_4$ + 5% NaCl solution at 35 and 70°C

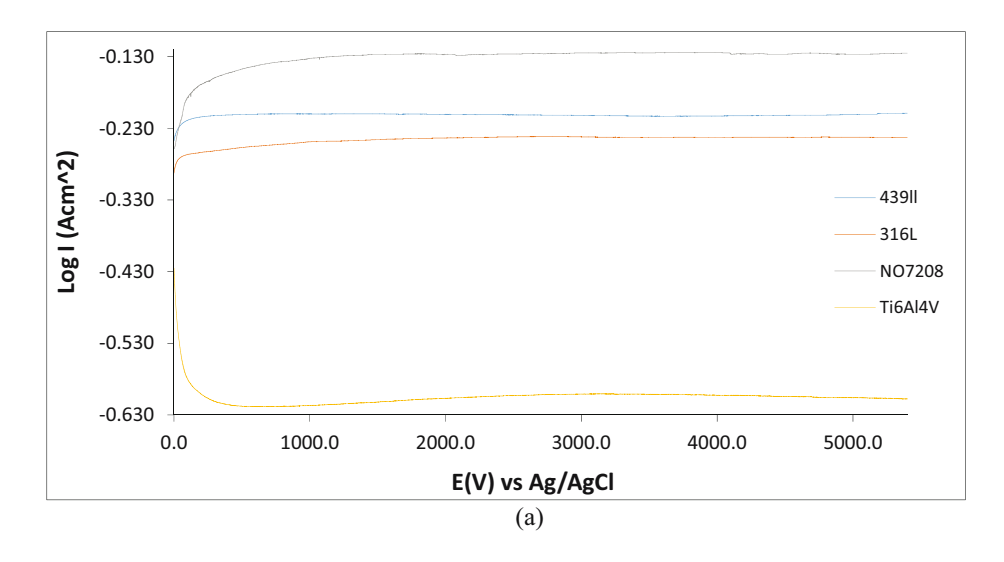
Alloy	C _P (V)	Metastable pitting potential (V)	Metastable pitting current (A)	Passivation potential (V)	Passivation current (A)	Pitting potential (V)	Pitting current (A)	Passivation range (V)
35°C								
NO7208	-0.235	0.02	3.05×10^{-4}	0.19	2.50×10^{-5}	1.04	3.30×10^{-5}	-0.17
Ti6Al4V	-0.496	-0.39	7.39×10^{-5}	-0.21	2.54×10^{-5}	I	I	I
70°C Ti6Al4V	-0.501	-0.41	2.80×10^{-3}	-0.13	1.62×10^{-4}	1	I	I

solution at 35 and 70°C with metastable pitting activity present. Metastable pits are transient corrosion pits which nucleate and grow for a few seconds before disappearing due to passivation of the steel at potentials less than the pitting potential [63]. At 35°C, Ti6Al4V and NO7208 exhibited metastable pitting behavior. Metastable pitting on Ti6Al4V polarization plot occurred at potential and current of -0.39 V and 7.39×10^{-5} A, respectively compared to NO7208 at 0.02 V and 3.05×10^{-4} A. This signifies that Ti6Al4V has a higher resistance to metastable pit formation compared to NO7208. This is further confirmed from the wider metastable pit region on the polarization plot of NO7208. Occurrence of metastable pitting on Ti6Al4V was gradual where there was a delayed transition. However, on NO7208, the transition was instantaneous over short potential range. Both alloys passivated at potentials of -0.21 and 0.19 V, and current of 2.50×10^{-5} and 2.54×10^{-5} A. At a potential of 1.04 V, stable pitting activity is obvious on the anodic polarization plot of NO7208, signifying breakdown of its protective oxide. However, this occurred almost instantaneously due to short transpassive behavior on the polarization plot [64,65]. The passivation range shows the resilience of NO7208 passive film before it collapses. In accordance with Machet et al. [66], the protective oxide on NO7208 consists of a furthermost film of Ni (OH)2, a middle film of Cr(OH)3, and an interior film of Cr₂O₃ oxide protecting the alloy. Passivation behavior was totally missing on the polarization plot of NO7208 alloy at 70°C. Increase in temperature of the electrolyte significantly influenced the stability of NO7208 passive film especially within the acid-chloride environments due to the accelerated agitation and diffusion of the reacting species [66–68]. According to Ahn et al. [69], reaction of corrosive anions with the protective oxide of NO7208 increases cation vacancies which are responsible for the collapse of its oxide. Ti6Al4V did not exhibit stable pitting activity throughout because of the strength of its protective oxide. However, the plot in Figure 1a shows that the passive film is marginally unstable. At 70°C, Ti6Al4V exhibited metastable pitting and passivation behavior. Metastable pitting occurred at -0.41 V and 2.80×10^{-3} A, while passivation due to the formation of stable TiO_2 occurred at -0.13 V and 1.62×10^{-4} A. The anodic polarization plot in Figure 1a and b, and the potentiostatic data show that Ti6Al4V does not pit, i.e., it undergoes localized corrosion degradation or stable pitting activity despite having the highest general C_R . TiO₂ remained resilient or in the active phase through formation of complex precipitates during potential scanning [70].

3.3 OCP analysis

OCP plots representing the active–passive transition behavior and thermodynamic corrosion tendency of 439ll, 316L, NO7208, and Ti6Al4V alloys in 4 M $\rm H_2SO_4$ + 5% NaCl solution at 35 and 70°C are displayed in Figure 2a and b. The OCP plots in Figure 2a and b confirms the C_R data of the alloys from potentiodynamic polarization. The plots show Ti6Al4V is the most electronegative with respect to the OCP plots of the other alloys [71]. At 35°C, Ti6Al4V OCP plot initiated at -0.425 V (0 s) and progressively decreased to cathodic potentials till -0.616 V at 400 s. Beyond this point relative thermodynamic balance was achieved till 5,400 s of exposure. At 70°C, Ti6Al4V plot started at -0.657 V (0 s) and culminated at -0.665 V (5,400 s) signifying higher corrosion tendency. Negligible potential

fluctuations are obvious on Ti6Al4V plot at 70°C compared to the plot at 35°C. Comparison of Ti6Al4V OCP plots at both temperatures show that increase in temperature increases the inclination of the alloys to corrode due to decrease in activation parameters for corrosion to occur. NO7208 plots were the most electropositive due to the growth and formation of its passive oxide, which significantly decreased its tendency to corrode [72-74]. At 35 and 70°C, the OCP plots initiated at -0.258 and -0.164 V, and culminated at -0.125 and -0.127 V representing marginal but increased tendency to corrode. 439ll and 316L were the intermediate plots with similar plot configuration at both temperatures due to similarity in the characteristics of the passive film evolved on the alloys during scanning. Increase in electrolyte temperature marginally increased the thermodynamic tendency of both steels to corrode.



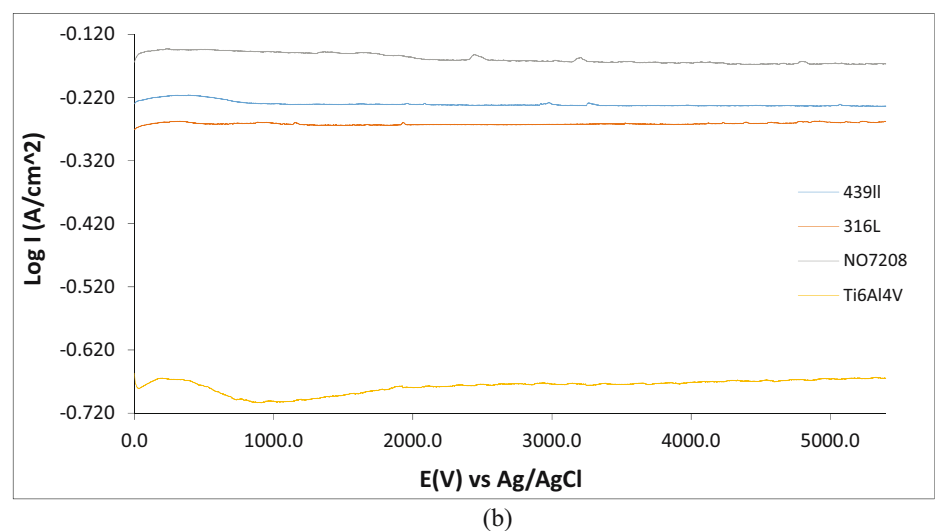


Figure 2: OCP plots of 439ll, 316L, NO7208, and Ti6Al4V alloys in 4 M $H_2SO_4 + 5\%$ NaCl solution at (a) 35°C and (b) 70°C.

518 — Roland Tolulope Loto DE GRUYTER

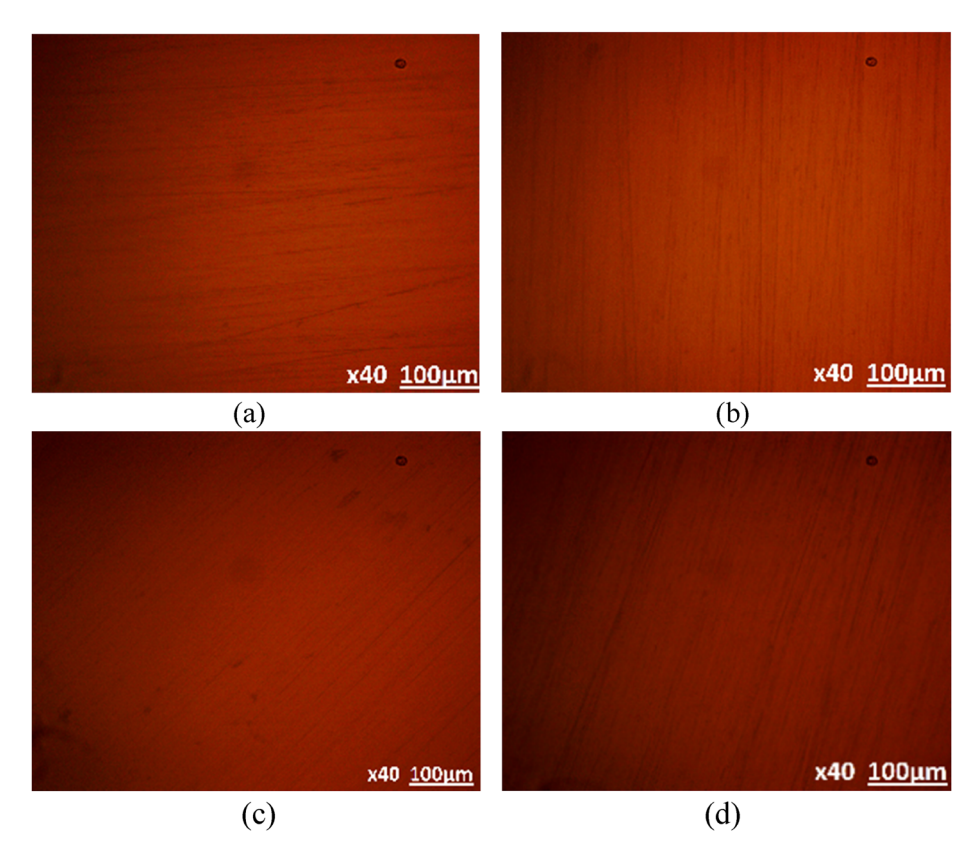


Figure 3: Optical morphology of (a) 439ll, (b) 316L, (c) NO7208, and (d) Ti6Al4V before corrosion test.

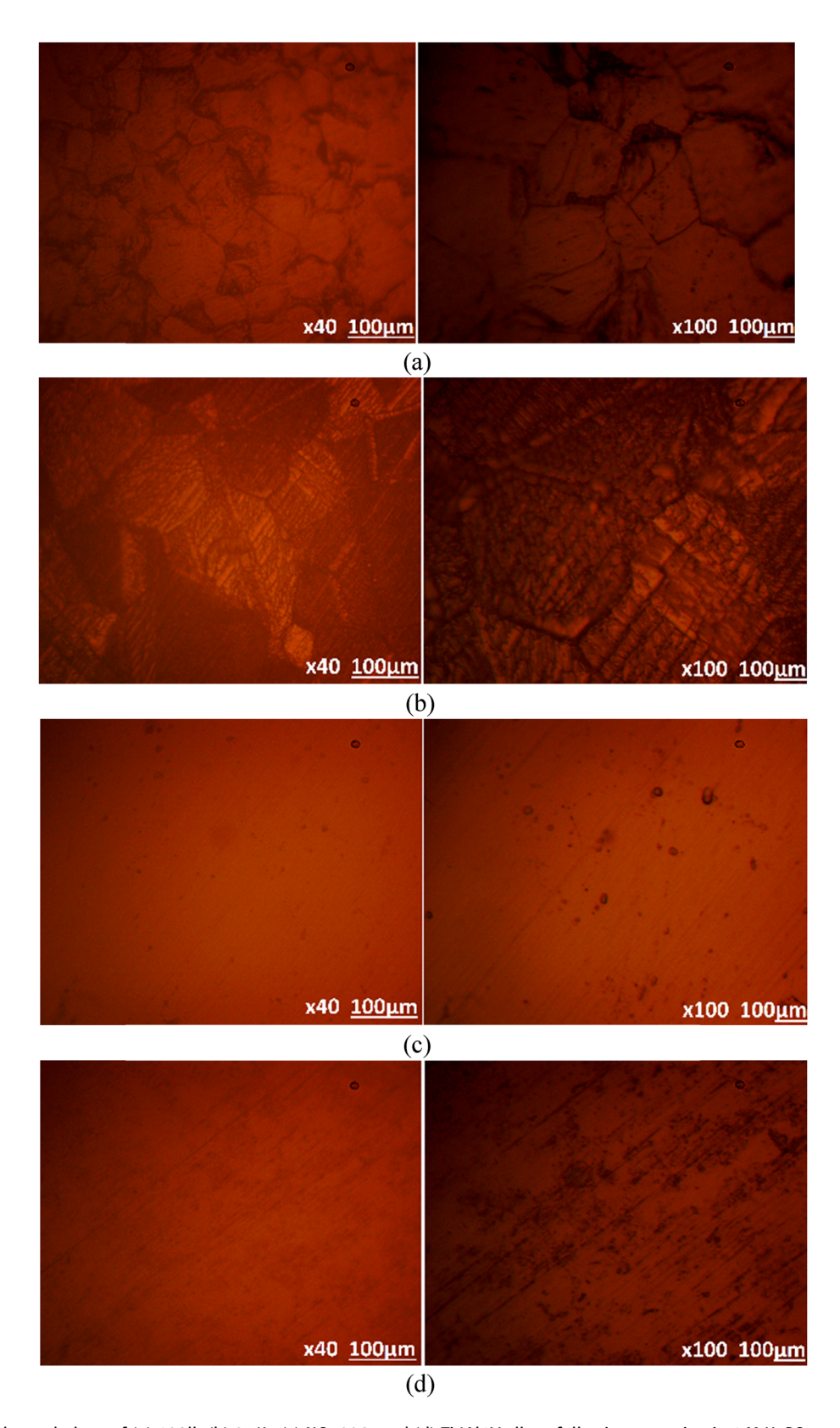
3.4 Optical microscopy characterization

The surface morphology of 439ll, 316L, NO7208, and Ti6Al4V metallic alloys prior to corrosion, and following corrosion at 35°C and at 70°C are laid out in Figures 3a–5d at magnitudes ×40 and ×100. The alloy morphologies before corrosion in Figure 3a-d are generally similar. However, Figure 4a-d presents morphological descriptions indicating corrosive wear which differ significantly from each other. The morphologies of 439ll and 316L in Figure 4a and b reveal the phase structures, grain boundaries, severe etching, and corrosion at the grain boundaries [75,76]. However, no obvious confirmation of pitting corrosion despite the presence of significant concentration of Cr content within the alloy microstructure. This signifies the total destruction of their protective oxide by the combined reactive nature of SO₄²⁻ and Cl⁻ anions inside the electrolyte, thus exposing the substrate alloy to accelerated general deterioration [77,78]. The morphology of NO7208 and Ti6Al4V (Figure 4c and d) shows that the protective film on their surface are resistant to deterioration although minor pseudo corrosion pits are obvious on NO7208, while the exterior of Ti6Al4V deteriorated slightly. At 70°C, the morphology of both alloys [Figure 5a–d] deteriorated severely.

Deterioration on 439ll, 316L, and Ti6Al4V appears to be general surface deterioration over the entire alloy surface, while on NO7208, deterioration occurred mostly at the grain boundaries in addition to etching of the surface.

4 Conclusion

NO7208 and 439ll stainless steel alloys exhibited the highest resistance to general corrosion at 35°C, while at 70°C NO7208 alloy was the most resistant. NO7208 and Ti6Al4V titanium alloy demonstrated sufficient resilience to localized corrosion due to resilience of their passive films as shown on the potentiodynamic polarization plot. While NO7208 and Ti6Al4V underwent metastable pitting activity at 35°C, only NO7208 pitted at a certain potential, while no pitting behavior occurred on Ti6Al4V. However, at 70°C, total destruction of the passive film on 439ll, 316L, and NO7208 alloys results in lack of passivation behavior, while Ti6Al4V passivated and did not pit during potential scanning. C_P of the alloys generally transited to higher cathodic values. OCP measurement showed NO7208 exhibited the most resilient passive film, while



 $\textbf{Figure 4:} \ \textbf{Optical morphology of (a) 439ll, (b) 316L, (c) NO7208, and (d) Ti6Al4V alloys following corrosion in 4 MH_2SO_4 + 5\% NaCl solution$ at 35°C.

520 — Roland Tolulope Loto DE GRUYTER

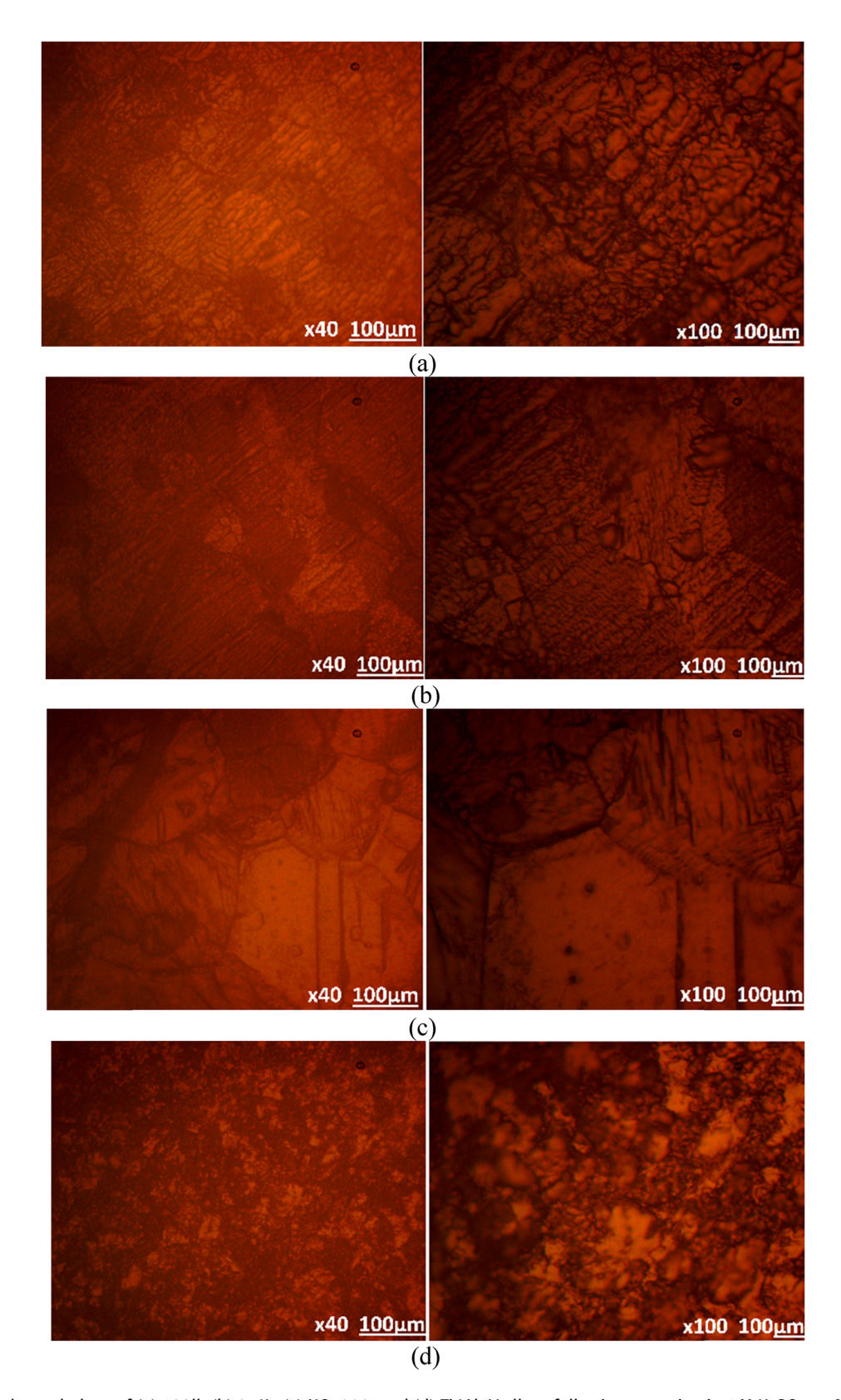


Figure 5: Optical morphology of (a) 439ll, (b) 316L, (c) NO7208, and (d) Ti6Al4V alloys following corrosion in 4 M $H_2SO_4 + 5\%$ NaCl solution at $70^{\circ}C$.

Ti6Al4V was the most electronegative. Optical images showed the microstructural properties of the alloys behave differently in the acid chloride environment. While deterioration of the alloys were along the grain boundaries, total surface deterioration was evident on Ti6Al4V alloy.

Acknowledgment: The author is thankful to Covenant University for their financial support towards this investigation.

Conflict of interest: Author states no conflict of interest exists

References

- Hoeppner DW, Arriscorreta CA. Exfoliation corrosion and pitting corrosion and their role in fatigue predictive modeling: state-of-the-art review. Int J Aerosp Eng. 2012;2012:1-2929. doi: 10.1155/2012/191879.
- Souza JCM, Henriques M, Teughels W, Ponthiaux P, Celis JP, Rocha LA. Wear and corrosion interactions on titanium in oral environment: literature review. J Bio Tribo Corros. 2015;1(13):13. doi: 10.1007/s40735-015-0013-0.
- Shaw BA, Kelly RG. What is corrosion? Electrochem Soc Interface. 2016;15(1):24-6.
- Marcus P, Maurice V. Materials science and engineering Vol. II, fundamental aspects of corrosion of metallic materials. Oxford, United Kingdom: EOLSS Publishers Co. Ltd.; 2014.
- [5] Topala P, Ojegov A, Besliu V. Formation of anticorrosive structures and thin films on metal surfaces by applying EDM. IntechOpen. 2019. doi: 10.5772/intechopen.80543.
- Carvalho ML. Corrosion of copper alloys in natural seawater: effects of hydrodynamics and pH; 2014. https://tel.archivesouvertes.fr/tel-01207012/document.
- Boillot P, Peultier J. Use of stainless steels in the industry: Recent and future developments. Procedia Eng. 2014;83:309-21. doi: 10.1016/j.proeng.2014.09.015.
- [8] Taban E, Kaluc E, Ojo OO. Properties, weldability and corrosion behavior of super martensitic stainless steels for on- and offshore applications. MP Mater Test. 2016;58(6):501-18.
- Mahato P, Mishra SK, Murmu M, Murmu NC, Hirani H, Banerjee P. A prolonged exposure of Ti-Si-B-C nano composite coating in 3.5 wt% NaCl solution: Electrochemical and morphological analysis. Surf Coat Tech. 2019;375:477-88.
- Kim SI, Lee HY, Song JS. A study on characteristics and internal exposure evaluation of radioactive aerosols during stainless pipe cutting in decommissioning of nuclear powerplant. Nucl Eng Technol. 2018;50(7):1088-98.
- [11] Reddy VS, Kaushik SC, Ranjan KR, Tyagi SK. State-of-the-art of solar thermal power plants—A review. Renew Sust Energ Rev.
- [12] Xiao G, Wang X, Zhang J, Ni M, Gao X, Luo Z, et al. Granular bed filter: A promising technology for hot gas clean-up. Powder Technol. 2013;244:93-9.

- [13] Rose L. On the degradation of porous stainless steel in low and intermediate temperature solid oxide fuel cell support materials. Electronic Theses and Dissertations, University of British Columbia. doi: 10.14288/1.0071732.
- [14] Tantawy N. Evaluation of new cationic surfactant as corrosion inhibitor for carbon steel in a metal working fluid. Ann Univ Dun area JOS Galat Fascicle. 2005;8:112-4.
- Beloglazov SM. Hydrogenation of steel in electrochemical [15] processes. Leningrad: Publishing House of the Leningrad University; 1975.
- [16] Bahadori A. Corrosion and materials selection: a guide for the chemical and petroleum industries. John Wiley & Sons, Ltd.; 2014. doi: 10.1002/9781118869215.
- [17] Seyeuxa A, Zannaa S, Allion A, Marcus P. The fate of the protective oxide film on stainless steel upon early stage growth of a biofilm. Corros Sci. 2015;91:352-6.
- [18] Baer DR. Protective and non-protective oxide formation on 304 stainless steel. Appl Surf Sci. 1981;7(1-2):69-82.
- [19] Loto RT, Loto CA. Corrosion behaviour of S43035 ferritic stainless steel in hot sulphate/chloride solution. J Mater Res Techn. 2018;7(3):231-9.
- [20] Loto RT. Effect of elevated temperature on the corrosion polarization of NO7718 and NO7208 nickel alloys in hot acid chloride solution. J Bio Tribo Corros. 2018;4(71):71.
- Heusler KE. Growth and dissolution of passivating films. Corr Sci. 1990;31:597-606.
- Outteridge T. Duplex stainless steel in pharmaceutical industry. http://www.sswnews.com/pdf/DuplexStainless Steel in Pharmaceutical Industry.pdf.
- [23] Loto RT, Loto CA. Potentiodynamic polarization behavior and pitting corrosion analysis of 2101 duplex and 301 austenitic stainless steel in sulfuric acid concentrations. J Fail Anal Preven. 2017;17(4):672-9.
- [24] Loto RT. Study of the corrosion resistance of type 304L and 316 austenitic stainless steels in acid chloride solution. Orient J Chem. 2017;33(3):1090-6.
- [25] Loto RT. Electrochemical corrosion characteristics of 439 ferritic, 301 austenitic, S32101 duplex and 420 martensitic stainless steel in sulfuric acid/NaCl solution. J Bio Tribo Corros. 2017;3(24).
- [26] Loto CA, Loto RT, Popoola API. Electrode potential monitoring of effect of plants extracts addition on the electrochemical corrosion behaviour of mild steel reinforcement in concrete. Int J Elect Sci. 2011;6(8):3452-65.
- [27] Loto RT. Comparative study of the pitting corrosion resistance, passivation behavior and metastable pitting activity of NO7718, NO7208 and 439L super alloys in chloride/sulphate media. J Mater Res Techn. 2019;8(1):623-9.
- ASTM G59-97. Standard test method for conducting potentio-[28] dynamic polarization resistance measurements; 2014. http:// www.astm.org/Standards/G31 [accessed: 06/04/21].
- ASTM G1-03. Standard practice for preparing, cleaning, and evaluating corrosion test specimens; 2011. http://www.astm. org/Standards/G1 [accessed: 06/04/21].
- [30] ASTM G102-89. Standard practice for calculation of corrosion rates and related information from electrochemical measurements; 2015e1. http://www.astm.org/Standards/G102.htm [accessed: 06/04/21].
- [31] Basics of corrosion measurements. http://www.che.sc.edu/ faculty/popov/drbnp/ECHE789b/Corrosion% 20Measurements.pdf [accessed: 06/04/21].

- [32] Loto CA, Loto RT, Popoola API. Synergistic effect of tobacco and kola tree extracts on the corrosion inhibition of mild steel in acid chloride. Int J Elect Sci. 2011;6(9):3830-43.
- [33] Sanjay KS. Basics of corrosion, in chemistry in green corrosion chemistry and engineering: Opportunities and challenges. Weinheim, Germany: Wiley-VCH Verlag GmbH & CoKGaA; 2012.
- [34] Zhang PQ, Wu JX, Zhang WQ, Lu XY, Wang K. A pitting mechanism for passive 304 stainless steel in sulphuric acid media containing chloride ions. Corros Sci. 1993;34(8):1343-9.
- [35] Okamoto G, Shibata T. Stability of passive stainless steel in relation to the potential of passivation treatment. Corros Sci.
- [36] Shehata OS, Lobna AK, Mandour HS. Effect of acetamide derivative and its mn-complex as corrosion inhibitor for mild steel in sulphuric acid. Egypt J Chem. 2017;60(2):243-59.
- [37] NBS Special Publication (Issues 476-479), United States. National Bureau of Standards, U.S. Government Printing Office, 1977.
- [38] Atapour M, Pilchak A, Frankel GS, Williams JC, Fathi MH, Shamanian M. Corrosion behavior of Ti-6Al-4V with different thermomechanical treatments and microstructures. Corrosion. 2010:66(6):065004-065004-9.
- [39] Raj B, Mudali UK. Materials development and corrosion problems in nuclear fuel reprocessing plants. Prog Nucl Energy. 2006;48(4):283-313.
- [40] Shu YH, Wang FH, Wu WT. Corrosion behavior of Ti60 alloy coated with a solid NaCl deposit in O2 plus water vapor at 500-700°C. Oxid Met. 1999;52:463-73.
- [41] Shu YH, Wang F, Wu WT. Synergistic effect of NaCl and water vapor on the corrosion of 1Cr-11Ni-2W-2Mo-V steel at 500-700°C. Oxid Met. 1999;51:97-110.
- [42] Shu YH, Wang FH, Wu WT. Corrosion behavior of pure Cr with a solid NaCl deposit in O2 plus water vapour. Oxid Met. 2000;54:457-71.
- [43] Dini C, Costa RC, Sukotjo C, Takoudis CG, Mathew MT, Barão VAR. Progression of bio-tribocorrosion in implant dentistry. Front Mech Eng. 2000;6:1-14.
- [44] Zhang L, Chen L. A review on biomedical titanium alloys: Recent progress and prospect. Adv Eng Mater. 2019;21:1801215.
- [45] Casillas N, Charlebois SJ, Smyrl WH, White HS. Scanning electrochemical microscopy of precursor sites for pitting corrosion on titanium. J Electrochem Soc. 1993;140:L142-5.
- [46] Casillas N, Charlebois SJ, Smyrl WH, White HS. Pitting corrosion of titanium. J Electrochem Soc. 1994;141:636-42.
- [47] Basame SB, White HS. Scanning electrochemical microscopy of native titanium oxide films mapping the potential dependence of spatially localized electrochemical reactions. J Phys Chem. 1995;99:16430-5.
- [48] Abd El Rehim SS, Hassan HH, Amin MA. Chronoamperometric studies of pitting corrosion on Al and Al-Si alloys by halide ions in neutral sulphate solutions. Corros Sci. 2004;46:1921-38.
- [49] Amin MA, Abd El Rehim SS, Moussa SO, Ellithy AS. Pitting corrosion of Al and Al-Cu alloys by ClO4 ions in neutral sulphate solutions. Electrochim Acta. 2008;53:5644-52.
- [50] McCafferty E. A competitive adsorption model for the inhibition of crevice corrosion and pitting. J Electrochem Soc. 1990;137:3731-7.
- [51] Dugdale I, Cotton JB. The anodic polarization of titanium in halide solutions. Corros Sci. 1964;4:397-411.

- [52] O'Grady WE, Roeper DF, Natishan PM. Structure of chlorine Kedge XANES spectra during the breakdown of passive oxide films on aluminium. J Phys Chem C. 2011;115(51):25298-303.
- [53] Mancia F. The effect of environmental modification on the sulphide stress corrosion cracking resistance of 13Cr martensitic stainless steel in H₂S-CO₂-Cl- systems. Corros Sci. 1987;27(10-11):1225-37.
- [54] Vitale D. Effect of hydrogen sulfide partial pressure, pH, and chloride content on the SSC resistance of martensitic stainless steels and martensitic precipitation hardening stainless steels. Houston, Texas: NACE International; 1999.
- [55] Hashizume S, Masamura K, Yamazaki K. Performance of high strength super 13% Cr martensitic stainless steels. Houston, Texas: NACE International: 2003.
- [56] Hoar T, Mears D, Rothwell G. The relationships between anodic passivity, brightening and pitting. Corros Sci. 1965;5(4):279-89.
- [57] Evans UR. The passivity of metals. Part I. The isolation of the protective film. J Chem Soc. 1927:1020-40.
- [58] McCafferty E, Kelly R, Frankel G, Natishan P, Newman R. Critical factors in localized corrosion III. Electrochem Soc Proc. 1999;98-17:42.
- [59] Heine M, Keir D, Pryor M. The specific effects of chloride and sulfate ions on oxide covered aluminium. J Electrochem Soc. 1965:112(1):24.
- [60] Richardson J, Wood G, Galvele JR. Transport processes and the mechanism of pitting of metals. J Electrochem Soc. 1976;123(4):464-74.
- [61] Hoar T. The production and breakdown of the passivity of metals. Corros Sci. 1967;7(6):341-55.
- [62] Burstein G, Mattin S, Natishan P, Kelly R, Frankel G, Newman R. The nucleation and early stages of growth of corrosion pits. Proceedings of the Symposium on Crit. Fact. Local Corros II. Pennington, Texas: The Electrochemical Society Inc., 1996;95-15:1-14.
- [63] Parangusan H, Bhadra J, Al-Thani N. A review of passivity breakdown on metal surfaces: influence of chloride- and sulfide-ion concentrations, temperature, and pH. Emergent Mater. 2021;4:1187-203. doi: 10.1007/s42247-021-00194-6.
- [64] Pistorius PC, Burstein GT. Metastable pitting corrosion of stainless steel and the transition to stability. Philos Trans R Soc A Philos T R Soc A. 1992;341:531-59.
- [65] Fattah-Alhosseini A, Attarzadeh N. The mechanism of transpassive dissolution of AISI 321 stainless steel in sulphuric acid solution. Int J Electrochem. 2011;2011:521384-9. doi: 10.4061/ 2011/521384.
- [66] Machet A, Galtayries A, Zanna S, Jolivet P, Foucault M, Combrade P, et al. Kinetics of passivation of a nickel-base alloy in high temperature water; 2007. https://inis.iaea.org/ collection/NCLCollectionStore/_Public/36/105/ 36105066.pdf.
- [67] Exbrayat L, Salaluk S, Uebel M, Jenjob R, Rameau B, Koynov K, et al. Nanosensors for monitoring early stages of metallic corrosion. ACS Appl Nano Mater. 2019;2(2):812-8.
- [68] Cardoso M, Amaral S, Martini E. Temperature effect in the corrosion resistance of Ni-Fe-Cr alloy in chloride medium. Corros Sci. 2008;50(9):2429-36.
- [69] Ahn S-J, Kwon H-S, Macdonald DD. Role of Chloride Ion in Passivity Breakdown on Iron and Nickel. J Electrochem Soc. 2005;152(11):B482.

- [70] Macdonald DD. Passivity the key to our metals-based civilization. Pure Appl Chem. 1999;71(6):951-78.
- [71] Karayan Al, Maya-Visuet E, Castaneda H. Transpassive behavior of UNS N08367 super austenitic stainless steel in LiBr solution. Corrosion. 2015;71(9):1110-20.
- [72] Zhang Y, Yang C, Zhao L, Zhang J. Study on the electrochemical corrosion behavior of 304 stainless steel in chloride ion solutions. Int J Electrochem Sci. 2021;16:210251. doi: 10.20964/2021.02.01.
- [73] El-Taib Heakal F, Ghoneim AA, Mogoda AS, Awad KM. Electrochemical behaviour of Ti-6Al-4V alloy and Ti in azide and halide solutions. Corros Sci. 2011;53:2728-37.
- [74] Oliveira NTC, Guastaldi AC. Electrochemical behavior of Ti-Mo alloys applied as biomaterial. Corros Sci. 2008;50:938-45.

- [75] El-Taib Heakal FE, Awad KA. Electrochemical corrosion and passivation behavior of titanium and its Ti-6Al-4V alloy in low and highly concentrated HBR solutions. Int J Electrochem Sci. 2011;6:6483-502.
- [76] Engelberg DL. Intergranular Corrosion, Reference Module in Materials Science and Materials Engineering. Shreir's Corros. 2010;2:810-27. doi: 10.1016/B978-044452787-5.00032-9.
- [77] Qi J, Huang B, Wang Z, Ding H, Xi J, Wantang Fu W. Dependence of corrosion resistance on grain boundary characteristics in a high nitrogen CrMn austenitic stainless steel. J Mater Sci Technol. 2017;33(12):1621-8.
- [78] Lyon S. 1 Overview of corrosion engineering, science and technology, nuclear corrosion science and engineering. Sawston, Cambridge: Woodhead Publishing Series in Energy; 2012. p. 3-30.